2024 IEEE International Conference on Robotics and Automation (ICRA 2024)
May 13-17, 2024. Yokohama, Japan

Robust Control for Bidirectional Thrust Quadrotors under Instantaneously Drastic Disturbances

Zujian Chen,[1,2] Shaolin Mo,[1] Botao Zhang[1] , Jiyu Li[3] and Hui Cheng*[1]

***Abstract*—Quadrotors may crash and cause severe accidents under instantaneously drastic disturbances. To mitigate the effect of such disturbances, these critical issues should be considered: efficient disturbance observation and compensation, full attitude controllability, and instant output power generation of the quadrotor. In this paper, to keep the quadrotor stable even under suddenly drastic disturbances, a novel control framework is presented to by integrating the advantages of active disturbance rejection control (ADRC) as well as geometric control for a quadrotor with bidirectional thrust capabilities. Moreover, to strengthen the adaptability under significant disturbances, a novel switching strategy is introduced into the control framework by virtue of the quadrotor's bidirectional thrust capabilities. The ADRC scheme is performed when the disturbances are within a range; alternatively, if the disturbances surpass the preset range and the desired control is beyond the ultimate output of the quadrotor, the quadrotor compliantly responds by executing a 180° flip reverse flight to handle such drastic disturbances. Numerical and real-world experiments demonstrate that the proposed robust control strategy has superior performance adapts to instantaneously drastic disturbances.**

***Index Terms*—Bidirectional Thrust Quadrotor, Suddenly Drastic Disturbances, Active Disturbance Rejection Control, Geometric Control, Model Predictive Control**

I. Introduction

Quadrotors have widespread applications for their remarkable mobilities. To facilitate the applications of the quadrotors, capabilities of environmental interactions and high mobility are required in drone racing [1]–[3] and aerial manipulation [4]–[8]. In such applications, instantaneously drastic disturbances may arise from unpredictable external forces in aerodynamic shifts [9] or dynamic environments [4], [10]. The quadrotors face increasing risks of crashes under such instant disturbances. Disturbance resistance is crucial to keep the quadrotors safe when performing high maneuvering and flexible aerial manipulation tasks. Major challenges in effectively handling such disturbances lie in achieving rapid and efficient disturbance observation and compensation, fully controlling attitude and generating instant output power of the quadrotor. quadrotors' disturbance observation and compensation have been proposed based on the classic Active Disturbance Rejection Control (ADRC) [11] scheme. In [12], the ADRC is integrated into the state-of-the-art cascaded control scheme for quadrotors. Both attitude loop and position loop disturbance rejection are considered. Zhao [13] put forth a novel control strategy for quadrotors, emphasizing an adaptation design for variable mass and active disturbance rejection. [14] showcased a multiple observers-based anti-disturbance control for quadrotors, specifically tailored to counter payload and wind disturbances. The external wrench uncertainty in the previously discussed tasks is relatively small. Moreover, they use Euler angles for attitude representation, which are then employed to estimate and compensate for disturbances. Such representation can lead to accumulated errors during continuous rotations. Furthermore, they predominantly focus on disturbance observation and compensation near the hovering state of quadrotors. In Cao's recent study [15], ESO-based tracking control was used for aerial manipulation with an unidirectional thrust quadrotor. Using a nonlinear attitude controller like [16] and trajectory planning considering the robotic arm's dynamic constraints, the delta arm mounted on the quadrotor, with a 1.2kg payload, achieved swift swinging motions with minimal tracking errors. The use of manipulator trajectory planning allows for a smoother torque variation in countering the flight platform. However, the challenge of addressing instantaneously drastic disturbances still requires further research. While the nonlinear attitude controller implemented by the author ensures controllability across all attitude orientations, it still leaves a gap in exploring disturbance observation and compensation under significant attitude tracking errors.

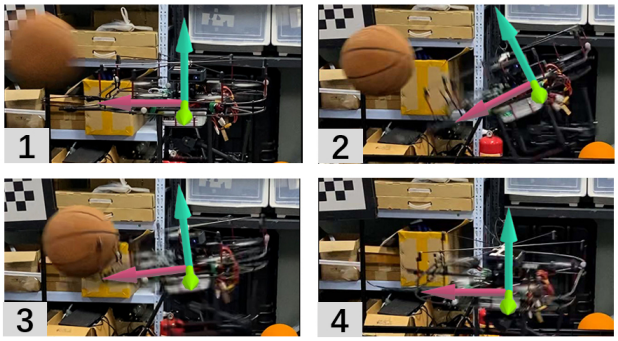

Fig. 1. Quadrotor resists impact and swiftly returns its stable state.

Methods that design controllers directly on geometric man-

This work was supported by the Science and Technology Program of Guangzhou under Grant 202206010164. *(Z. J. Chen and S. L. Mo contributed equally to this work.) (Corresponding Author: Hui Cheng.)*

[1]Z. J. Chen, S. L. Mo, B. T. Zhang and H. Cheng are with the School of Computer Science and Engineering, Sun Yat-sen University, Guangzhou 510006, China.

[2]Z. J. Chen is also with the College of Mechatronics and Control Engineering, Shenzhen University, Shenzhen 518060, China.

[3]J. Y. Li is with the College of Engineering, South China Agricultural University, Guangzhou 510642, China.

ifolds [16], [17] are coordinate-free. Consequently, they can ensure controllability across all attitude orientations. Lee et al. [16] formulated a controller on the nonlinear configuration Lie group,avoiding singularities and complexities that arise when using local coordinates. Their approach demonstrated the capability to achieve exponential stability when the initial attitude error is less than 90° and almost global exponentially attractiveness when the initial attitude error is less than 180°. However, few studies on geometric control consider the observation and compensation of disturbances, particularly instantaneously drastic ones.

In recent years, by utilizing symmetric propellers and modern ESCs, the bidirectional thrust capability of a quadrotor has been enabled [18]–[21]. Such capability not only doubles the control torque envelope, enhancing maneuverability, but also permits reversed flight in specific scenarios—all without the need for additional actuators that might compromise flight endurance. Moreover, the symmetric propellers design provides a great potential to handle instantaneously drastic disturbances by leveraging the bidirectional thrust capabilities. The bidirectional thrust has yet to be applied to mitigate drastic disturbances.

In this paper, by exploiting the potential of bidirectional thrust and flip maneuver ability of symmetric propellers quadrotor, a novel control framework is presented for quadrotors under instantaneously drastic disturbances. The main contributions of our work are summarized as follows:

- Instantly drastic disturbances on the quadrotors will cause its large attitude deviation. An attitude control method based on geometric manifolds and ADRC is proposed to keep the quadrotor stable even under large attitude deviation. In addition, a parameterized approach to generate spherical reference trajectories with varying dynamical properties is introduced, allowing the attitude tracking performance of the quadrotors to be tailored to specific requirements.
- To ensure that our quadrotor remains maneuverability even under significant disturbances, a novel switching strategy is proposed, leveraging the quadrotor's bidirectional thrust capabilities, which either generate greater torque or facilitate reversed flight. The ADRC scheme is performed if the disturbances are within a range. On the other hand, when the disturbances surpass the preset range(it implies that the desired control is beyond the ultimate output of the quadrotor), the quadrotor compliantly responds by executing a 180° flip maneuver to handle such drastic disturbances.

The switching strategy represents an intriguing and practical attempt to mitigate the risk of quadrotor crashes. It is noteworthy that in this paper, the threshold is assumed to be constant and is preset based on the observed disturbance and the upper limit of the quadrotor's thrust output.

This paper is organized as follows: Section II presents the dynamics of the bidirectional thrust quadrotor. Section III presents the control strategy. Experimental validations and analyses are introduced in Section IV. Conclusion and future work are discussed in Section V. The main symbols used in this paper are listed in Table I.

TABLE I
OVERVIEW OF THE MAIN SYMBOLS USED IN THIS PAPER

Symbol	Definition
$\boldsymbol{\mathcal{F}_W}$, $\boldsymbol{\mathcal{F}_B}$	World Inertial Frame, quadrotor Body Frame
m, $\mathbf{I_v}$	Vehicle's mass, inertia
$\boldsymbol{g}$	Gravity acceleration
$\mathbf{p}, \mathbf{v}, \mathbf{a}$	Pos., vel., acc. of O_B in $\mathcal{F}_W$
$\mathbf{R}$	Rotation matrix of $\mathcal{F}_B$ w.r.t. $\mathcal{F}_W$
$\mathbf{b1}$, $\mathbf{b2}$, $\mathbf{b3}$	The first, second and third column of matrix $\mathbf{R}$
$\boldsymbol{\Omega^B}$,$\dot{\boldsymbol{\Omega}}^{\boldsymbol{B}}$	Angular vel., acc. in $\mathcal{F}_B$
$\mathbf{f}_i^B$	Force on CoM by the i^{th} actuator
$\mathbf{e_z}$	Unit Vector $[0,0,1]^T$
$\boldsymbol{f_\xi}$, $\boldsymbol{\tau_\xi^B}$	External force, torque on CoM
$\boldsymbol{d_i^B}$	Position vector of the i^{th} actuator in $\mathcal{F}_B$
$\boldsymbol{M}$	Allocation matrix of quadrotor
$\boldsymbol{u}_{tran}$, $\boldsymbol{u}_{rot}$	Fully-actuated control input of rigid body
$\boldsymbol{u_{flat}}$	Flat control input of quadrotor
$\boldsymbol{l_\Omega}$	Observer bandwidth specific to angular vel.
$\boldsymbol{w}$, $\boldsymbol{w_d}$	rotors angular vel. and desired rotors angular vel.
c_{t_+}, c_{t_-}	CW and CCW thrust coefficients of propellers
$\hat{\boldsymbol{\Omega}}^{\boldsymbol{B}}$	Observer's current estimation of angular vel. in $\mathcal{F}_B$
$\boldsymbol{a_{min}}$, $\boldsymbol{a_{max}}$	Acc. constraints in $\mathcal{F}_W$
$\boldsymbol{\tau_{min}}$, $\boldsymbol{\tau_{max}}$	Torque constraints in $\mathcal{F}_B$
$\mathbf{R}^\times$	The reduced matrix of $\mathbf{R}$, 2×2
$\mathbf{R}_{:,3}$	The third column of matrix $\mathbf{R}$
$\mathbf{v}_{1:2}$	The first two elements of vector $\mathbf{v}$

II. BIDIRECTIONAL THRUST QUADROTOR DYNAMIC

The translational dynamics of the quadrotor are represented within the inertial reference frame $\mathcal{F}_W$, while the rotational dynamics are characterized within the body-fixed reference frame $\mathcal{F}_B$. Utilizing the Newton-Euler equation, the dynamics are captured as follows:

$$\sum_{i=1}^{4} \boldsymbol{R f_i^B} + \boldsymbol{f_\xi} + m\boldsymbol{g} = m\boldsymbol{a} \tag{1}$$

$$\sum_{\boldsymbol{i=1}}^{\boldsymbol{4}} \boldsymbol{f_i^B} \times \boldsymbol{d_i^B} + \boldsymbol{\tau_\xi^B} - \boldsymbol{\Omega^B} \times \boldsymbol{I_v \Omega^B} = \boldsymbol{I_v \dot{\Omega}^B} \tag{2}$$

A distinctive feature of the bidirectional thrust quadrotor is that it can produce both positive and negative forces aligned with the body's z-axis. For the i-th thrust within frame $\mathcal{F}_B$, it can be expressed as:

$$\boldsymbol{f_i^B} = h(w_i)\boldsymbol{e_z}, \quad h\left(w_i\right) = \begin{cases} c_{t_+} w_i^2 & w_i \geq 0 \\ c_{t\_} w_i^2 & w_i < 0 \end{cases} \tag{3}$$

Equation (3) underscores the distinction between the bidirectional and unidirectional thrust quadrotor models by representing thrust in both forward and reverse motor rotations. The Fully-actuated control input $\boldsymbol{u} = [\boldsymbol{u_{tran}}, \boldsymbol{u_{rot}}]^{\boldsymbol{T}}$ is defined as:

$$\begin{cases} \boldsymbol{u}_{tran} = \sum_{i=1}^{4} h\left(w_i\right) \boldsymbol{R e_z} \\ \boldsymbol{u}_{rot} = \sum_{i=1}^{4} h\left(w_i\right) \boldsymbol{e_z} \times \boldsymbol{d_i^B} \end{cases} \tag{4}$$

Given that the quadrotor is an underactuated system and its dynamics are recognized as differentially flat [22], the control input can be represented in 4-dimension, yielding:

$$\boldsymbol{u_{flat}} = \left[\boldsymbol{u}_{rot}^T, \sum_{i=1}^{4} h\left(w_i\right)\right]^T \tag{5}$$

The correlation between the desired control input and the anticipated rotational speed of each actuator is given by:

$$\boldsymbol{u_{flat}} = \boldsymbol{M}\boldsymbol{h}(\boldsymbol{w}) \tag{6}$$

The matrix $\boldsymbol{M}$ characterizes the quadrotor's physical attributes, detailed in [23], which is invertible, hence obtained:

$$\boldsymbol{h}(\boldsymbol{w}) = \boldsymbol{M}^{-1}\boldsymbol{u_{flat}} \tag{7}$$

III. Control Strategy

In this section, we employ the classic cascaded framework, integrating extended states observer (ESO), model predictive control (MPC), and geometric control methods. An overview of this control framework is illustrated in Fig.2.

A. Uncertainties Estimation and Compensation

To observe and compensate the uncertain disturbances, a second-order linear ESO [24] is utilized for the attitude loop.

$$\begin{aligned} \dot{\hat{\boldsymbol{\Omega}}}^{\boldsymbol{B}} &= \boldsymbol{I_v^{-1}}(\boldsymbol{u_{rot}} + \boldsymbol{\tau_\xi^B}) + \boldsymbol{2l_\Omega}(\boldsymbol{\Omega^B} - \hat{\boldsymbol{\Omega}}^{\boldsymbol{B}}) \\ \dot{\boldsymbol{\tau}}_{\boldsymbol{\xi}}^{\boldsymbol{B}} &= \boldsymbol{I_v l_\Omega^2}(\boldsymbol{\Omega^B} - \hat{\boldsymbol{\Omega}}^{\boldsymbol{B}}) \end{aligned} \tag{8}$$

The paper focuses on the attitude control, and it simply assumed $\boldsymbol{f_\xi}$ to be consistently zero to ensure uniformity in the dynamic formulation.

B. Position Control

We adopt a LMPC approach for position control inspired by the method presented in [25]. This is utilized to facilitate the performance analysis of attitude control during flight. The position control is based on a fundamental translation model, expressed as follows:

$$\begin{cases} \boldsymbol{p(k+1)} = \boldsymbol{p(k)} + \Delta t \cdot \boldsymbol{v(k)} + 0.5 \cdot \Delta t^2 \cdot \boldsymbol{a(k)} \\ \boldsymbol{v(k+1)} = \boldsymbol{v(k)} + \Delta t \cdot (\boldsymbol{a(k)}) \\ \boldsymbol{u_{tran}(k)} = m(\boldsymbol{a(k)} - \boldsymbol{g}) - \boldsymbol{f_\xi(k)} \end{cases} \tag{9}$$

Hard constraint for optimization is defined as follows:

$$m\boldsymbol{a_{min}} \leq \boldsymbol{R_0^T u_{tran}(k)} \leq m\boldsymbol{a_{max}}, \quad k = 0, \ldots, N-1 \tag{10}$$

where R_0^T is the transpose of R_0, representing the rotation measured at the current time. Compared to the reference methods, our hard constraints incorporate the term R_0^T. This inclusion ensures that the acceleration in translation aligns more closely with the quadrotor's characteristics.

The desired control input for translation can be obtained by solving the following Optimal Control Problem:

$$\begin{aligned} \min_{\boldsymbol{p},\boldsymbol{v},\boldsymbol{u_{tran}}} \sum_{k=0}^{N-1} \Big(\|\boldsymbol{e_p}(k)\|^2_{\boldsymbol{Q_p}} + \|\boldsymbol{e_v}(k)\|^2_{\boldsymbol{Q_v}} + \|\boldsymbol{u(k)_{tran}}\|^2_{\boldsymbol{Q_{ut}}} \Big) \\ + \|\boldsymbol{e_p(N)}\|^2_{\boldsymbol{P_p}} + \|\boldsymbol{e_v(N)}\|^2_{\boldsymbol{P_v}} \\ \text{subject to} \quad (9)(10) \end{aligned} \tag{11}$$

where $\boldsymbol{e_p} = \boldsymbol{p_d} - \boldsymbol{p}$, and $\boldsymbol{e_v} = \boldsymbol{v_d} - \boldsymbol{v}$.

Finally, a control command for the low-level controller can be obtained [16]:

$$\boldsymbol{b3_d} = \frac{\boldsymbol{u_{tran}}}{\|\boldsymbol{u_{tran}}\|}, \quad T_d = \boldsymbol{u_{tran}} \cdot \boldsymbol{b3} \tag{12}$$

Combined with a desired yaw angle, the desired rotation matrix $\boldsymbol{R_d}$ can be computed [16].

Algorithm 1: Geometric Attitude Control

Init Data:
  $\boldsymbol{LKT} \leftarrow$ TrajectoryGeneration() (Algorithm 2)
while *Quadrotor is in operation* **do**
  Update Desired Orientation:
    $\boldsymbol{R_d} \leftarrow$ position_controller
  Update Sensor Inputs:
    $\boldsymbol{R} \leftarrow$ sensor_mocap
    $\boldsymbol{\Omega^B} \leftarrow$ sensor_imu
  Retrieve Raw Trajectory:
    $\boldsymbol{b3} \leftarrow (\boldsymbol{R_d^T R})_{:,3}$
    $\boldsymbol{Trajseg} \leftarrow Segment(\boldsymbol{LKT}, \boldsymbol{b3}, N)$
  Calculate Correction Matrix:
    $\boldsymbol{e_{b3}} = \boldsymbol{b3} - \tilde{\boldsymbol{b3}}_{\boldsymbol{d}}$
    $\boldsymbol{torsion} = \frac{\boldsymbol{e_{b3}}_{1:2}}{\|\boldsymbol{e_{b3}}_{1:2}\|}$
    $\boldsymbol{b1} = [\boldsymbol{torsion}^T, \boldsymbol{0}]^T$
    $\boldsymbol{b2} = \boldsymbol{b1} \times \boldsymbol{e_z}$
    $\boldsymbol{R_{cor}} = [\boldsymbol{b1}, \boldsymbol{b2}, \boldsymbol{e_z}]$
  Calculate Corrected Trajectory:
  for $i = 1$ **to** N **do**
    $\boldsymbol{trajSeg_{cor}}[:, i] \leftarrow \boldsymbol{R_{cor}}\boldsymbol{trajSeg}[:, i]$
  MPC Solution:
    $\boldsymbol{u_{rot}} \leftarrow SolveMPC()$ (13 ~ 15)

C. Geometric Attitude Control

We propose a method for attitude control on geometric manifolds, capitalizing on its inherent coordinate-free nature. The target for attitude tracking is denoted as $\tilde{\boldsymbol{b3}}_{\boldsymbol{d}} = [0, 0, 1]^T$, representing a consistent, coordinate-independent unit vector. In our approach, the attitude control focuses on determining the initial condition for MPC prediction iteration and a segment of a dynamically feasible spherical reference trajectory for tracking. This ensures the quadrotor attains the desired orientation by resolving the MPC problem and commanding the result to the actuators. The segment of a dynamically feasible spherical reference trajectory is obtained by searching within a lookup table (LKT). Further details about the initial condition and trajectory segment will be discussed later in this section. The proposed geometric attitude control method is illustrated in Algorithm 1.

*1) **Rotational Dynamics Feasible Spherical Trajectory**:* We generate a global reference trajectory that is invariant to coordinates, spanning the vector $\boldsymbol{b3}$ from $[0, \epsilon, \epsilon - 1]^T$ to $[0, 0, 1]^T$. The inclusion of ϵ facilitates a proper initiation for spherical interpolation. Using the $fhan$ function [11], we ensure smooth and consistent interpolation between these vectors, setting a dynamically feasible trajectory for attitude tracing. This trajectory is visualized in Fig. 3, and the details of trajectory generation method appear in Algorithm 2. Given that the spherical trajectory covers from $-\pi/2$ to $\pi/2$, a reference for flip maneuvers is always available, ensuring robust attitude tracking. Moreover, dynamic adjustment of the LKT offers diverse tracking performances, either more

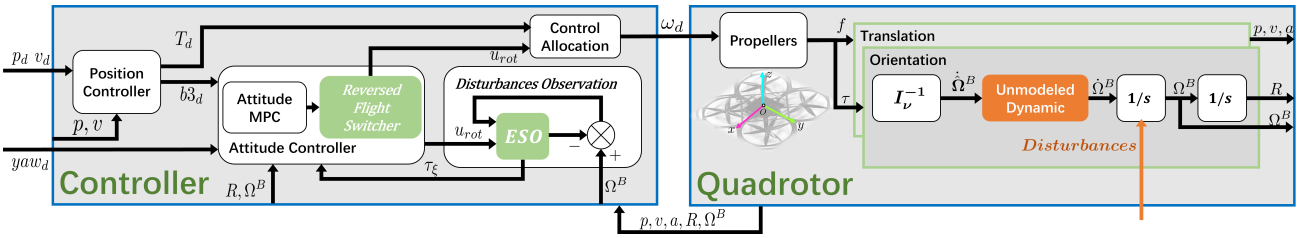

Fig. 2. An overview of the proposed control framework for a bidirectional thrust quadrotors under disturbances.

Algorithm 2: Spherical Trajectory Generation

Init Data:
  $\boldsymbol{b3_d} \leftarrow [0,0,1]^T, \quad \boldsymbol{b3} \leftarrow [0,\epsilon,\epsilon-1]^T$
  $\theta \leftarrow 0.0 \quad \dot{\theta} \leftarrow 0.0$
while $\theta \leq \pi$ **do**
  Compute Interpolation $b3$ **Via** $fhan$**:**
    $fh \leftarrow fhan(\theta-\pi, \dot{\theta}, r, h0)$
    $\dot{\theta} \leftarrow \dot{\theta} + h \times fh$
    $\theta \leftarrow \theta + h \times \dot{\theta}$
    $\boldsymbol{b3_{intermid}} \leftarrow \frac{\sin(\pi-\theta)\boldsymbol{b3}+\sin(\theta)\boldsymbol{b3_d}}{\|\sin(\pi-\theta)\boldsymbol{b3}+\sin(\theta)\boldsymbol{b3_d}\|}$
  Append to Lookup Table:
    $\boldsymbol{LKT} \xleftarrow{\text{append}} \boldsymbol{b3_{intermid}}$

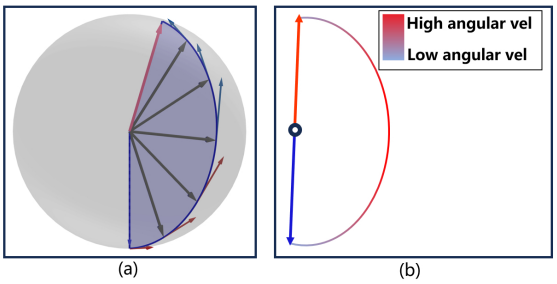

Fig. 3. (a) 3D visualization of the spherical trajectory: arcs represent the trajectory, tangents on the arcs indicate angular velocity, and unit vectors represent $\boldsymbol{b3}$ at different moments. (b) 2D visualization of the spherical trajectory utilizes color gradation, where darker shades signify higher angular velocity, while lighter shades represent lower angular velocity.

aggressive or energy-efficient. Algorithm 2 presents a highly parameterized approach, allowing for dynamic trajectory updates within a single control cycle. Adjusting the dynamic factor r and the smoothing factor h_0 allows for efficiently tailoring the spherical trajectory.

By employing the lookup table and a sliding window mechanism, we can capture the primary characteristics of rotation, circumventing the complex nonlinear computations inherent in rotation problems.

*2) **Reduced Attitude Representation for MPC**:* The method for controlling the yaw angle is adapted from [16]. In this work, the simplified rotation model is specifically formulated to emphasize tilt tracking, as described by:

$$\begin{cases} \boldsymbol{b3}(k+1) = \boldsymbol{b3}(k) + (\boldsymbol{\Omega}(k) \times \boldsymbol{b3_d}(k)) \cdot \Delta t \\ \boldsymbol{\Omega}(k+1)_{1:2} = \boldsymbol{\Omega}(k)_{1:2} + \dot{\boldsymbol{\Omega}}(k)_{1:2} \cdot \Delta t \\ \dot{\boldsymbol{\Omega}}(k)_{1:2} = \boldsymbol{I_v^{-1}}^{\times}(\boldsymbol{u_{rot}}(k)_{1:2} + \boldsymbol{\zeta}(k)) \\ \boldsymbol{\zeta}(k) = (\boldsymbol{\Omega_d}(k) \times \boldsymbol{I_v}\boldsymbol{\Omega}(k) + \boldsymbol{\tau_\xi^B}(k))_{1:2} \end{cases} \tag{13}$$

In the first row of this equation, the angular acceleration term is not incorporated into the integration of $\boldsymbol{b3}$. In the forth row of this equation, the desired angular velocity (which is assumed to be a pre-defined constant) is utilized to simplify the optimization problem when addressing operations associated with the cross-product. Meanwhile, it's imperative to note that ζ is a two-dimensional vector, and formulates without considering the influence of yaw angle acceleration.

For our OCP problem, the hard constraints are defined as follows:

$$\boldsymbol{\tau_{min}} \leq \boldsymbol{u_{rot}(k)} \leq \boldsymbol{\tau_{max}}, \quad k = 0, \ldots, N-1 \tag{14}$$

The desired control input can be obtained by solving the following:

$$\begin{aligned} \min_{\boldsymbol{b3},\boldsymbol{\Omega},\boldsymbol{u_{rot}}} \sum_{k=0}^{N-1} \Big(& \|\boldsymbol{e_{b3}}(k)\|^2_{\boldsymbol{Q_{b3}}} + \|\boldsymbol{e_\Omega}(k)\|^2_{\boldsymbol{Q_\Omega}} + \|\boldsymbol{u(k)_{rot}}\|^2_{\boldsymbol{Q_{ur}}} \Big) \\ & + \|\boldsymbol{e_{b3}}(N)\|^2_{\boldsymbol{P_{b3}}} + \|\boldsymbol{e_\Omega}(N)\|^2_{\boldsymbol{P_\Omega}} \\ & \text{subject to} \quad (13)(14) \end{aligned} \tag{15}$$

where $\boldsymbol{e_{b3}} = \tilde{\boldsymbol{b3}}_{\boldsymbol{d}} - \boldsymbol{b3}$ denotes attitude error in reduced representation, and $\boldsymbol{e_\Omega} = (\boldsymbol{R^T R_d \Omega_d} - \boldsymbol{\Omega^B})_{1:2}$ represents angular velocity error in pitch and roll channel.

*3) **Reversed Flight Switching**:* The details for representing attitude in normal flight and reversed flight are found in [26]. Our main focus is on determining the triggering strategy for the flip maneuver. It triggers only when the following two criteria are simultaneously met: 1. The estimated angular disturbance acceleration exceeds a predetermined threshold; 2. The current motor speed approaches its maximum rotational capacity. Through this triggering strategy, we effectively determine whether external disturbances exceed the tolerable range for the quadrotor and then execute operations with minimal risk. In this work, we set these two thresholds at $60\,\text{rad/s}^2$ and 90% of the maximum motor speed, respectively.

IV. Experiment

To validate the attitude tracking capability of the bidirectional thrust quadrotor under our control strategy, we design tasks that include response to step commands and continuous flips (Fig. 4(a)(b)(c)). To further validate our system's ability

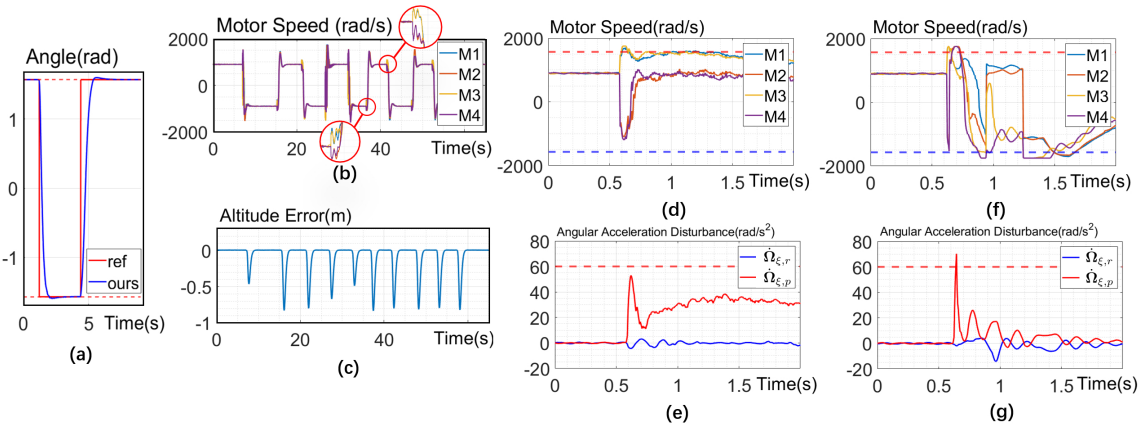

Fig. 4. (a): Bidirectional thrust Quadrotor's attitude tracking during two 180° flips. The first transition is from $\pi/2$ (vertically upwards) to $-\pi/2$ (vertically downwards), followed by the reverse. The y-axis represents the tilting angle between the z-axis of $\mathcal{F}_B$ and the xy-plane of $\mathcal{F}_W$. (b): Motor speed curves during continuous flips of the quadrotor. Notable discrepancies are observed in the flips during the 25~35s interval, characterized by frequent motor speed fluctuations. (c): Altitude tracking errors during quadrotor flipping maneuvers. The drops in altitude correspond to the moments of each flip. (d)(e): Bidirectional thrust Quadrotor's resilience upon collision with a 1 kg sphere dropped from 1m above. After regaining stability, all motor speeds are in the positive direction. (f)(g): Bidirectional thrust Quadrotor executes a compliant flip upon collision with a 1 kg sphere dropped from 2m above. After regaining stability, all motor directions turn to the negative direction. The dashed lines represent the set thresholds.

to resist unknown disturbances and its adaptability, we design the impact resilience test (Fig. 4(d)(e)) and the impact compliant response test (Fig. 4(f)(g)). For further confirmation of efficacy and practical significance, we design a similar impact resilience experiment in real flight (Fig. 6). In the simulation, the quadrotor we use has a mass of 2.3 kg, with a moment of inertia defined as diag$[0.083, 0.083, 0.1]$, and a diagonal motor distance of 0.42 m. In the real flight experiments, the quadrotor we use weighs 2.5 kg and has a diagonal motor distance of 0.34 m. The Opti-Track motion capture system and the Pixhawk V6X flight controller are utilized.

A. Simulation

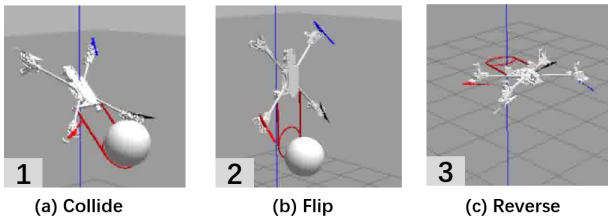

Fig. 5. Snapshots of the quadrotor's flip behavior in numerical simulations.

*1) **Attitude Tracking and Continuous Flip Ability**:* In the experiments presented, the quadrotor's attitude tracking response to step commands evaluates and is illustrated in Fig. 4(a). The initial maneuver highlights the quadrotor's transition from an orientation of $\pi/2$ (vertically upwards) to $-\pi/2$ (vertically downwards). During this transition, the quadrotor completes approximately 90% of the 180° flip within 510ms, with an overshoot of less than 2% throughout the entire process. Subsequently, the quadrotor is commanded to transition from $-\pi/2$ back to $\pi/2$. The response duration remains consistent at approximately 500ms, with a similar overshoot of under 2%. The consistent performance of the quadrotor, even during challenging maneuvers, highlights the strength and dependability of our attitude control approach. Additionally, the minimal overshoot observed underscores its ability to stabilize efficiently after a maneuver, laying the foundation for subsequent experiments and practical applications. In Fig. 4(b), the motor speed curves during continuous flips show the behavior of the control effectiveness of our approach. The swift transition of motor speed from positive to negative, or inversely, demonstrates that our controller effectively harnesses the potential of the bidirectional thrust quadrotor. At the start of each flip, there is acceleration in a pair of motors and deceleration in the other set, generating torque for the flipping motion. Towards the end of the flip, a change in motor speeds can be observed, which indicates the counter-torque applied for the quadrotor's stabilization post-flip. Within the 25-35s timeframe, variations in the motor speed patterns are observed. This could be due to the noise introduced in the simulation and a transient unstable state. The controller responds by adjusting the motor speeds to achieve post-flip stability. As depicted in Fig. 4(c), the altitude changes experienced by the quadrotor consistently tie to its flipping maneuvers. Corresponding to each flip, there is a pronounced decline in altitude, averaging around 0.6m. The minimal descent in altitude is attributed to the swiftness of our flip maneuver.

*2) **Instantaneously Drastic Disturbances Resilience and Compliant Behaviors**:* In this experiment, a 1 kg sphere drops from a height of 1m to 2m above the quadrotor to induce an instantaneously drastic disturbance. The sphere eventually collides with the edge of the bidirectional thrust quadrotor's body. Trigger thresholds detailed in Section III-C are set as follows for this simulation: 1. The maximum rotational speed is 1750 rad/s, with 90% of this value being 1575 rad/s; 2. The disturbance magnitude threshold is 60 rad/s^2. The compliant flip only performs when both thresholds are surpassed.

As depicted in Fig. 4(e), the ESO data reveals that between 0.5s to 1s, a disturbance with an angular acceleration of up to 50 rad/s^2 is detected. This disturbance curve indicates

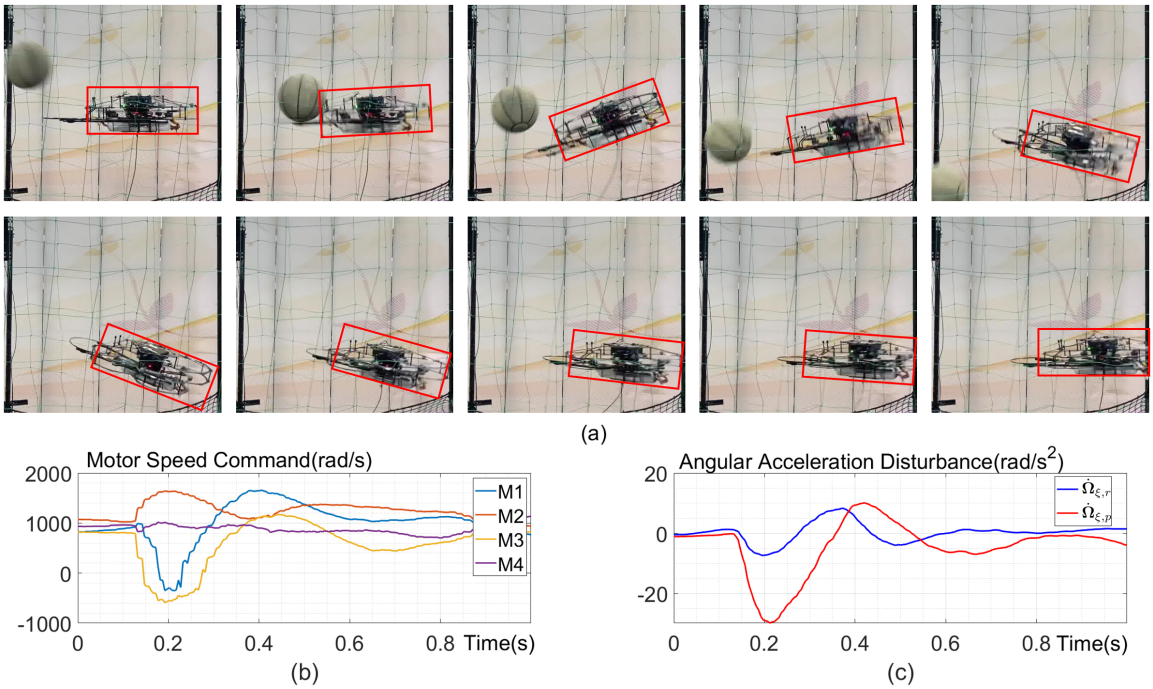

Fig. 6. (a): The snapshots of the quadrotor's resilience behavior when the edge of the quadrotor is hit by a basketball. (b): The motor speed response of quadrotor during the impact. (c): The observed angular acceleration disturbance by ESO.

that post-collision, the disturbance initially peaks and then stabilizes. This stabilization is attributed to the quadrotor capturing the sphere and, under the influence of gravity, the consequent wrench exerted on the quadrotor. Correspondingly, Fig. 4(d) showcases the control response of the bidirectional thrust quadrotor to this disturbance. Between 0.5s to 1s, our system reacts swiftly. Motors M2 and M4 quickly reverse direction, while M1 and M3 increase their speed in the positive direction, consistent with the control allocation inherent to the bidirectional thrust quadrotor. This immediate adjustment in motor speeds exemplifies our approach's efficiency. The eventual stabilization of motor speeds indicates that instantaneously drastic disturbances are successfully counteracted.

In Fig. 4(f), the motor speed curves for the bidirectional thrust quadrotor reveal its distinctive compliant flip behavior in the face of instantaneously drastic disturbances. The activation of this compliant flip arises when both the motor speeds and the disturbance magnitude, as observed by the ESO, surpass the predetermined threshold. Between 0.5s to 1.5s, the quadrotor initiates this flip. In response, the motors promptly reverse their rotation direction, producing a control torque that aligns with the angular acceleration disturbance's direction. This coordinated torque assists the Bidirectional thrust Quadrotor in executing a 180° flip, minimizing potential uncontrollable risks.

B. Real-World Flight Experiment

In the real-world experiments, the abilities of the bidirectional thrust quadrotor to resist instantaneously drastic disturbances are validated by throwing a 600g basketball to hit the edge of the quadrotor. As shown in Fig. 6(b), when the quadrotor is hit by a basketball on its edge, it rapidly generates greater torque by reversing its motors. It indicates that the proposed controller effectively utilizes the bidirectional thrust capabilities of the quadrotor. Fig. 6(c) shows the observed angular acceleration disturbance of approximately 30 rad/s^2, which corresponds to the moment of collision as captured in Fig. 6(a). Real-world experimental results demonstrate that the proposed control method effectively adapts to the instant and huge impact of basketball. It is noted that the disturbance observation and compensation respond to the instant disturbances more slowly in reality compared to simulations. The discrepancy may be due to the communication and control latency, as well as the phase lag in angular velocity when performing IMU signal filtering.

V. Conclusion

In this paper, a novel control framework for quadrotors is proposed to handle instantaneous drastic disturbances. It innovatively integrates the benefits of the geometric method with ADRC for a bidirectional thrust quadrotor to deal with the large attitude deviation caused by instantly drastic disturbances. Moreover, a novel switching strategy is presented leveraging the quadrotor's reversed flight capabilities to enhance its adaptability to drastic disturbances. The numerical simulation experiments illustrate the superior performance of the proposed control framework adaptive to instantaneously drastic disturbances. In real-world experiments, the bidirectional thrust quadrotor can withstand sudden and huge impacts from a 600g basketball, even when it is struck on the edge of the quadrotor. In the future work, the switching strategy and flipping maneuvers adapted to instantly drastic disturbances will be further studied and applied to real-world flights.

REFERENCES

[1] Y. Song, M. Steinweg, E. Kaufmann, and D. Scaramuzza, "Autonomous drone racing with deep reinforcement learning," in *Proc. IEEE/RSJ Int. Conf. Intell. Robot. Syst.*, 2021, pp. 1205–1212.

[2] C. Pfeiffer, S. Wengeler, A. Loquercio, and D. Scaramuzza, "Visual attention prediction improves performance of autonomous drone racing agents," *Plos one*, vol. 17, no. 3, p. e0264471, 2022.

[3] E. Kaufmann, L. Bauersfeld, A. Loquercio, M. Müller, V. Koltun, and D. Scaramuzza, "Champion-level drone racing using deep reinforcement learning," *Nature*, vol. 620, no. 7976, pp. 982–987, 2023.

[4] A. Ollero, M. Tognon, A. Suarez, D. Lee, and A. Franchi, "Past, present, and future of aerial robotic manipulators," *IEEE Trans. Robot.*, vol. 38, no. 1, pp. 626–645, 2021.

[5] Z. Ouyang, R. Mei, Z. Liu, M. Wei, Z. Zhou, and H. Cheng, "Control of an aerial manipulator using a quadrotor with a replaceable robotic arm," in *Proc. IEEE Int. Conf. Robot. Autom.*, 2021, pp. 153–159.

[6] M. Brunner, G. Rizzi, M. Studiger, R. Siegwart, and M. Tognon, "A planning-and-control framework for aerial manipulation of articulated objects," *IEEE Robot. Autom. Lett.*, vol. 7, no. 4, pp. 10 689–10 696, 2022.

[7] M. Xu, A. Hu, and H. Wang, "Image-based visual impedance force control for contact aerial manipulation," *IEEE Trans. Automat. Sci. Eng.*, vol. 20, no. 1, pp. 518–527, 2022.

[8] G. Garimella, M. Sheckells, S. Kim, G. Baraban, and M. Kobilarov, "Improving the reliability of pick-and-place with aerial vehicles through fault-tolerant software and a custom magnetic end-effector," *IEEE Robot. Autom. Lett.*, vol. 6, no. 4, pp. 7501–7508, 2021.

[9] H. Huang, G. M. Hoffmann, S. L. Waslander, and C. J. Tomlin, "Aerodynamics and control of autonomous quadrotor helicopters in aggressive maneuvering," in *Proc. IEEE Int. Conf. Robot. Autom.*, 2009, pp. 3277–3282.

[10] P. Lassen and M. Fumagalli, "Can your drone touch? exploring the boundaries of consumer-grade multirotors for physical interaction," in *Proc. IEEE Int. Conf. Robot. Autom.*, 2022, pp. 1–7.

[11] J. Han, "From pid to active disturbance rejection control," *IEEE Trans. Ind. Electron.*, vol. 56, no. 3, pp. 900–906, 2009.

[12] Y. Zhang, Z. Chen, X. Zhang, Q. Sun, and M. Sun, "A novel control scheme for quadrotor uav based upon active disturbance rejection control," *Aerosp. Sci. Technol.*, vol. 79, pp. 601–609, 2018.

[13] J. Zhao, X. Ding, B. Jiang, G. Jiang, and F. Xie, "A novel control strategy for quadrotors with variable mass and external disturbance," *Int. J. Robust Nonlinear Control*, vol. 31, no. 17, pp. 8605–8631, 2021.

[14] K. Guo, J. Jia, X. Yu, L. Guo, and L. Xie, "Multiple observers based anti-disturbance control for a quadrotor uav against payload and wind disturbances," *Control Eng. Pract.*, vol. 102, p. 104560, 2020.

[15] H. Cao, Y. Li, C. Liu, and S. Zhao, "Eso-based robust and high-precision tracking control for aerial manipulation," *IEEE Trans. Autom. Sci. Eng.*, 2023.

[16] T. Lee, M. Leok, and N. H. McClamroch, "Geometric tracking control of a quadrotor uav on se (3)," in *Proc. IEEE 49th Conf. Decis. Control*, 2010, pp. 5420–5425.

[17] Y. Yu, S. Yang, M. Wang, C. Li, and Z. Li, "High performance full attitude control of a quadrotor on so (3)," in *Proc. IEEE Int. Conf. Robot. Autom.*, 2015, pp. 1698–1703.

[18] M. Maier, "Bidirectional thrust for multirotor mavs with fixed-pitch propellers," in *Proc. IEEE/RSJ Int. Conf. Intell. Robot. Syst.*, 2018, pp. 1–8.

[19] W. Jothiraj, C. Miles, E. Bulka, I. Sharf, and M. Nahon, "Enabling bidirectional thrust for aggressive and inverted quadrotor flight," in *Proc. Int. Conf. Unmanned Aircraft Syst.*, 2019, pp. 534–541.

[20] W. Jothiraj, I. Sharf, and M. Nahon, "Control allocation of bidirectional thrust quadrotor subject to actuator constraints," in *Proc. Int. Conf. Unmanned Aircraft Syst.*, 2020, pp. 932–938.

[21] J. Wehbeh and I. Sharf, "An mpc formulation on $so(3)$ for a quadrotor with bidirectional thrust and nonlinear thrust constraints," *IEEE Robot. Autom. Lett.*, vol. 7, no. 2, pp. 4945–4952, 2022.

[22] D. Mellinger and V. Kumar, "Minimum snap trajectory generation and control for quadrotors," in *Proc. IEEE Int. Conf. Robot. Autom.*, 2011, pp. 2520–2525.

[23] J. C. Monteiro, F. Lizarralde, and L. Hsu, "Optimal control allocation of quadrotor uavs subject to actuator constraints," in *Proc. Amer. Control Conf.*, 2016, pp. 500–505.

[24] Z. Gao *et al.*, "Scaling and bandwidth-parameterization based controller tuning," in *Proc. Amer. Control Conf.*, 2003, pp. 4989–4996.

[25] M. Kamel, M. Burri, and R. Siegwart, "Linear vs Nonlinear MPC for Trajectory Tracking Applied to Rotary Wing Micro Aerial Vehicles," in *Proc. IFAC-PapersOnLine 20th IFAC World Congr.*, 2017, pp. 3463–3469.

[26] K. Mao, J. Welde, M. A. Hsieh, and V. Kumar, "Trajectory planning for the bidirectional quadrotor as a differentially flat hybrid system," in *Proc. IEEE Int. Conf. Robot. Autom.*, 2023, pp. 1242–1248.